Journal of Alloys and Compounds 506 (2010) 739–744

Contents lists available at ScienceDirect

Journal of Alloys and Compounds

journal homepage: www.elsevier.com/locate/jallcom

Synthesis and characterization of nano-crystalline $Ce_{1-x}Gd_xO_{2-x/2}$ ($x = 0$–0.30) solid solutions

L.D. Jadhav[a,*], M.G. Chourashiya[b], A.P. Jamale[b], A.U. Chavan[b], S.P. Patil[b]

[a] Department of Physics, Rajaram College, Kolhapur 416004, India
[b] Department of Physics, Shivaji University, Kolhapur 416004, India

ARTICLE INFO

Article history:
Received 30 April 2010
Received in revised form 6 July 2010
Accepted 7 July 2010
Available online 15 July 2010

Keywords:
Ceramics
Chemical synthesis
Infrared spectroscopy
Raman spectroscopy
Microstructure

ABSTRACT

In recent years, doped ceria is an established and promising candidate as solid electrolyte for intermediate temperature solid oxide fuel cell (IT-SOFC). In this investigation, synthesis and characterizations of nano-crystalline Gd doped ceria, ($Ce_{1-x}Gd_xO_{2-x/2}$, where $x = 0$–0.3), prepared using glycine–nitrate process (GNP) has been presented. Evolution of structural and morphological properties of nano-powders as a function of heat treatment has also been studied. The prepared samples were characterized using TG–DTA, FT-IR, Raman spectroscopy, XRD, SEM, etc. In addition, the effect of Gd content over the micro-structural properties of nano-crystalline Gd doped ceria was investigated. Raman analysis of calcined powders confirms the formation of the solid solution of $Ce_{1-x}Gd_xO_{2-x/2}$ instead of mixture of CeO_2 and Gd_2O_3. The solid solutions obeyed Vegard's rule very well. Grain growth of sintered samples was observed to hinder with an increase in Gd content.

1. Introduction

Ceria (CeO_2), which possesses the fluorite structure, can be readily doped with trivalent cationic oxides (M_2O_3). This doped ceria becomes a good oxygen-ion conductor, since in doped ceria due to charge compensation mechanism in host lattice, the oxygen vacancies ($V_O^{\cdot\cdot}$) are introduced. These oxygen vacancies are largely responsible for oxygen-ion conductivity. For example, ceria doped with gadolinia (Gd_2O_3) produces oxygen vacancies by the reaction

$$Gd_2O_3 + 2Ce_{Ce}^{\times} + O_O^{\times} \rightarrow 2Gd_{Ce}' + V_O^{\cdot\cdot} + 2CeO_2 \quad (1)$$

Moreover, higher oxygen-ion conductivity of doped ceria than that of its competent material has made it a promising candidate for a variety of electrochemical devices, for example, as solid electrolytes for intermediate temperature solid oxide fuel cell (IT-SOFC) [1], three way catalysts for the treatment of automotive exhaust gases [2], petroleum cracking catalyst [3], oxygen sensors [4], UV filter [5], etc. In the recent past years due to this commercial drive to prepare ceria-based devices, many research articles in literature are dedicated to prepare the doped ceria by variety of methods [6–12]. However, due to various problems encountered in standard procedure of preparation of doped ceria, the clear understanding of preparation of doped ceria is essential. For long time, the standard procedure to obtain highly dense doped ceria as solid electrolyte for SOFC was to sinter the green compacts at high temperature ($\geq$1500 °C). However, main drawback of high temperature processing of doped ceria has been observed to cause reduction of Ce^{4+} to Ce^{3+}, giving electronic conduction. This electronic conduction leads to failure of fuel cell reaction. In addition, the high temperature processing is an expensive option of manufacturing. Moreover, it would not be suitable for the case of anode supported SOFC where the co-firing of the anode and electrolyte is necessary and may lead to inter-diffusion of unwanted cations.

In general, sintering promotes densification due to grain growth either by surface diffusion, grain boundary diffusion or by lattice diffusion which in turn depends upon the employed sintering temperature. It has been well explained by Espositow and Traversa [13] and suggested that the size of the starting material affects the sintering rate. According to Espositow and Traversa nano-sized particles as starting material promote low temperature sinterability and increases sintering rate due to their high surface energy. Therefore, use of nano-powders of doped ceria as starting material would be a good practice to obtain highly dense samples at comparatively low sintering temperatures.

Among the various solution routes available for the preparation of nano-oxide materials, the solution combustion, (e.g. glycine–nitrate process—GNP), is a versatile route. The benefits and advantages of this synthesis technique have been reported elsewhere [14,15]. Being a solution process, atomic level doping and homogeneity can be achieved [16]. In the present paper, we report the preparation of Gd doped ceria, ($Ce_{1-x}Gd_xO_{2-x/2}$), where Gd content was varied at the interval of 0.05.The nano-powders were used

* Corresponding author. Tel.: +91 9890694409; fax: +91 0231 2691533.
E-mail address: ldjadhav.phy@gmail.com (L.D. Jadhav).

0925-8388/$ – see front matter © 2010 Elsevier B.V. All rights reserved.
doi:10.1016/j.jallcom.2010.07.058

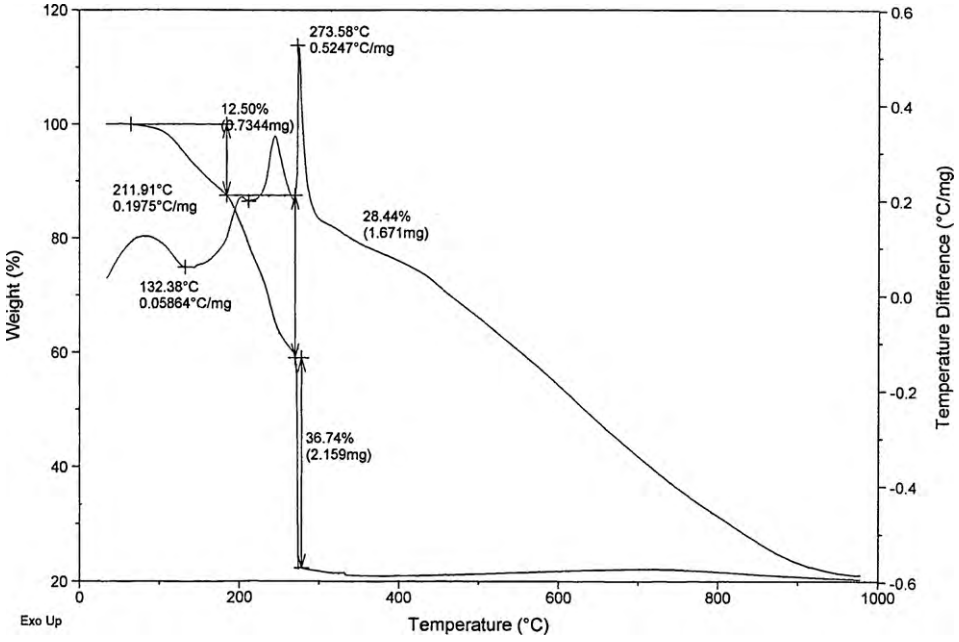

Fig. 1. Plot of TG–DTA of the gel formed during synthesis of 10% Gd doped ceria nano-powders.

to obtain ceramic samples which were sintered at different sintering temperature to decide the optimum sintering temperature. Further the effect of Gd content over the structural and morphological properties of nano-crystalline Gd doped ceria was investigated.

2. Experimental

2.1. Sample preparations

The fuel-to-oxidizer is an important preparative parameter of glycine–nitrate process. Our earlier work was dedicated to optimization of fuel-to-oxidizer ratio of GNP to obtain good quality Gd doped ceria nano-powders [14]. The optimized fuel-to-oxidizer ratio obtained from earlier work was 1.66:1. The chemical reaction for this fuel-to-oxidizer would be

$$Ce(NO_3)_3 6H_2O + 1.66C_2H_5NO_2 \xrightarrow{\Delta > 1500\,^\circ C} CeO_2 + 2.33N_2 + 3.32CO_2 + 10.15H_2O \quad (2)$$

In solution combustion reactions, extremely high temperatures of over 1550 °C can be achieved within a very short duration. Therefore, a thermally isolated system exists as there would be very little time to disperse the heat to its surroundings. Accordingly, the maximum temperature obtained during the reaction is assumed to be adiabatic temperature (T_{ad}). The heat liberated during the reaction is the enthalpy of the system and is a state function. It is expressed as

$$\Delta H^0 = \int_{298\ K}^{T_{ad}} n\Delta C_p(\text{product})\,dT \quad (3)$$

where n is the number of the moles, T is the adiabatic flame temperature and ΔH is enthalpy of combustion, which is given as

$$\Delta H = \Delta H_{product} - \Delta H_{Reactant} \quad (4)$$

Table 1
Enthalpy and specific heat at constant pressure of different species involved in reaction given by Eq. (2).

Compound	ΔH (kcal/mol)	C_p (kcal/mol K) at 298 K
$Ce(NO_3)_3{\cdot}6H_2O$	−729.14	–
$C_2H_5NO_2$	−112.20	–
CeO_2	−260.20	0.01473
N_2	0.00	0.00679
CO_2	−94.05	0.01115
H_2O	−57.80	0.00827

Table 1 lists the enthalpy and specific heat at constant pressure of different species involved in reaction given by Eq. (2). From Table 1 and Eq. (4) ΔH for reaction

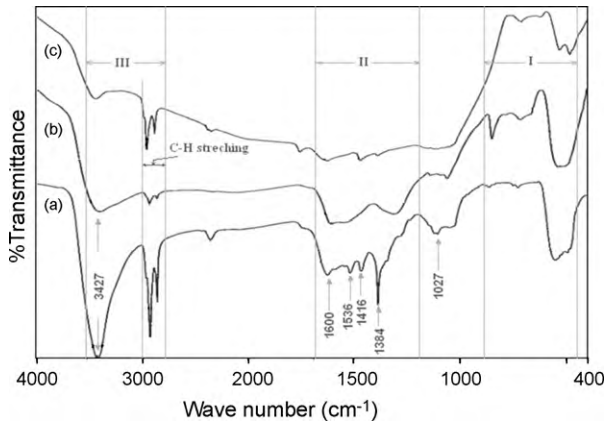

Fig. 2. FT-IR of (a) as-synthesized, (b) calcined and (c) sintered (1200 °C) 10% Gd doped ceria.

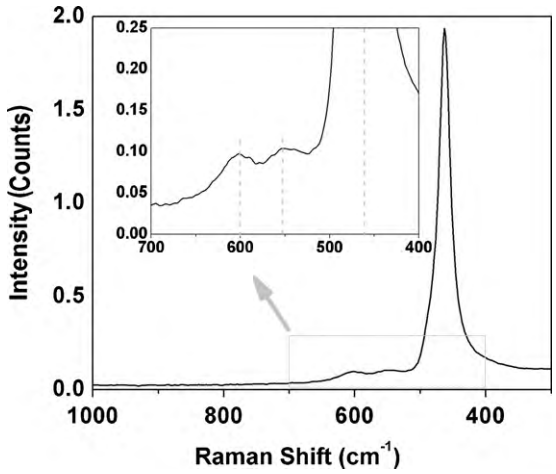

Fig. 3. Raman spectra of Gd doped ceria powder.

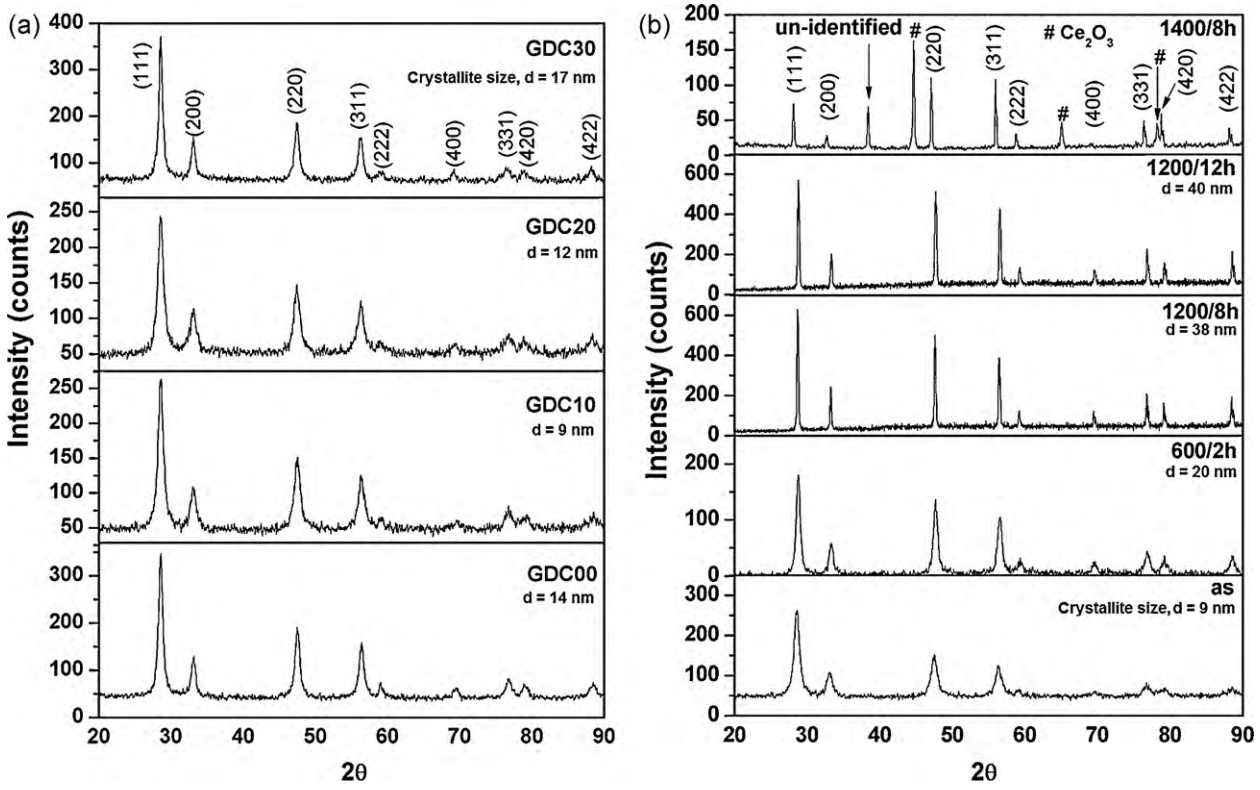

Fig. 4. XRD patterns of (a) as-synthesized un-doped and Gd doped ceria samples and (b) 10% Gd doped ceria samples heat treated at different temperatures.

mentioned in Eq. (2) is

$$\Delta H = -915.408268 - (1159.116) = -243.7077\ \text{kcal/mol}$$

Now

$\sum(nC_p)$=Summation of specific heats (at constant pressure) of reaction products

Again from Table 1

$$\sum(nC_p) = 0.15158\ \text{kcal/mol K}$$

Solving the Eq. (3) for T_{ad}, we get

$$T_{ad} = 298 + \left(\frac{-\Delta H}{\sum(nC_p)}\right) = 1905.81\ \text{K} = 1607\ ^\circ\text{C}$$

However, the actual flame temperatures will be much lower (±100 °C) than the theoretically calculated values, as the radiative losses, incomplete combustion and heating of air may cause the reduction. Despite of these losses, the adiabatic flame temperature at which the reactants are raised during the combustion is much higher than the decomposition temperature (<350 °C) of $Ce(NO_3)_3{\cdot}6H_2O$ [14]. Hence, glycine–nitrate combustion produces the nano-powders of ceria despite the short duration (i.e., few seconds) of auto-ignition. XRD of as-synthesized powders clearly reveals that the GNP is a single-step synthesis technique to produce phase-pure nano-crystalline powders.

To synthesize nano-powders of $Ce_{1-x}Gd_xO_{2-x/2}$ (where x = 0–0.30; Δ = 0.05) using glycine–nitrate combustion route, the metal nitrates (cerium nitrate and gadolinium nitrate; ALFA AESAR, 99.9%) and glycine was mixed in pre-optimized fuel-to-oxidizer ratio. The doping of Gd in ceria was controlled by varying blending proportion of respective metal nitrates in oxidizing precursors. This mixture was heated on hot plate with constant stirring, until formation of the gel. The gel was then transformed to a muffle-furnace, preheated at 325 °C. After few seconds, the gel auto-ignites with evolution of voluminous gases. During this short exposure of high temperature, formation of solid solution of GDC takes place. Heating was continued for a while so that un-burn part is completely burned. The nano-particles thus obtained have high surface area (73 m^2/g) and soft agglomerates (D_{50} = 5.34 μm) [14]. These powders were then calcined at 600 °C/2 h to burn the un-burned residual organic matter (if any).

2.2. Characterizations

Prior to powder synthesis thermo-gravimetric and differential thermal analysis (TG–DTA) of dried gel was carried out using a Perkin-Elmer TGA–DTA–DSC instrument with a heating rate of 10 °C/min in air to investigate the reaction temperature and to observe the behavior of material with temperature. The prepared nano-powders were characterized by Fourier transformed infrared (FT-IR) spectroscopy using 'Perkin-Elmer, FT-IR spectrum one' for detection of various phases. Raman spectroscopy was also performed and the spectra were collected at room temperature (FT-Raman, MultiRAM). The phase formation of samples was examined with powder X-ray diffractometer (XRD-PHILIPS PW-3710). The surface morphological properties of the sintered pellets were investigated using scanning electron microscopy (JEOL-JSM-6360) which further employed for determination of grain size, using Cottrell's method. The Cottrell's method gives the relation between the number of intercepts of the grain boundary per unit length (P), and total number of

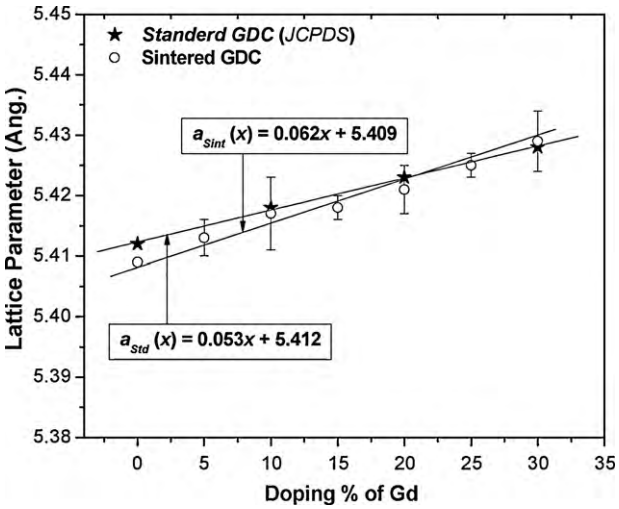

Fig. 5. Dependence of lattice parameter on doping % of Gd in ceria for standard (from JCPDS) and sintered GDC samples.

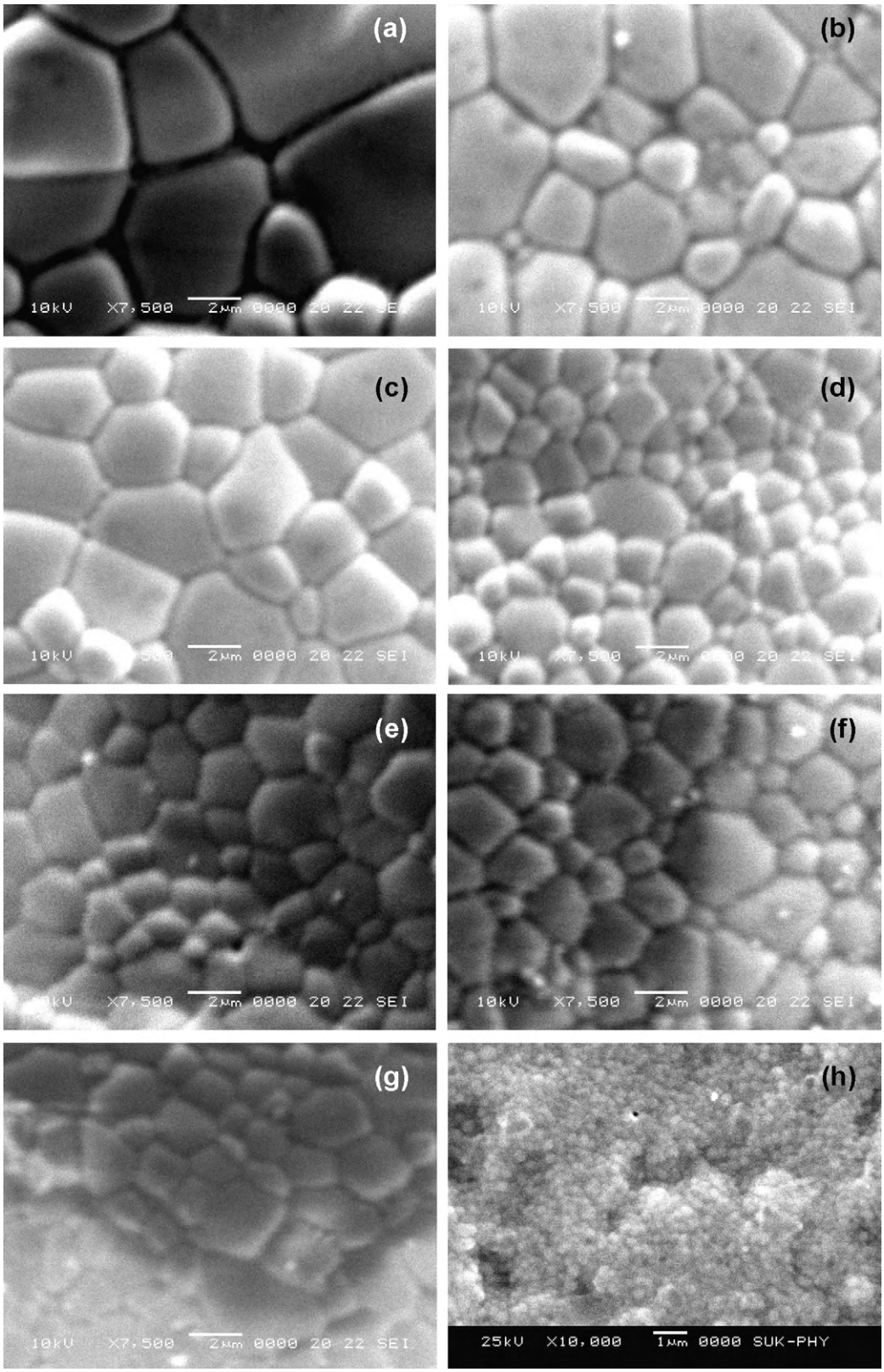

Fig. 6. SEM images of (a) un-doped, (b) 5% Gd doped, (c) 10% Gd doped, (d) 15% Gd doped, (e) 20% Gd doped, (f) 25% Gd doped and (g) 30% Gd doped ceria samples sintered at 1400 °C. (h) SEM image of 10% Gd doped ceria sintered at 1200 °C (8 h).

intercept (n) as, $P=(n/2\Pi r)M$, where M is the magnification and r is the radius of circle. Using P, grain diameter (L) can be calculated as, $L=1/(P-1)$.

3. Results and discussion

3.1. Thermo-gravimetric and differential thermal analysis (TG–DTA)

Fig. 1 shows the TG–DTA plot of the gel formed after dehydration of mixture of metal nitrates and glycine (for 10% Gd doped ceria—GDC10). The TG–DTA revealed the ignition and phase formation temperatures. The TGA plot showed two major weight losses in the range 60–210 °C and 210–300 °C. The presence of an endothermic peak and two exothermic peaks in DTA curve accompany the weight loss in the TGA.

The gradual weight loss in the range from 60 to 210 °C and the presence of an endothermic peak at 132.38 °C is attributed to the dehydration of gel. The steep reduction in sample weight, above 210 °C, is due to decomposition of the gel. During steep reduction in sample weight two exothermic peaks are observed in DTA, a small peak followed by pronounced one at 273.58 °C. Earlier may correspond to the combustion of the residual organic matter in the dehydrated sample while later would be due to the change of cerium oxide structure from an amorphous state to a crystalline state. An absence of any weight loss in TGA and endothermic or exothermic peak in DTA curve above 300 °C confirms formation of fluorite type $Ce_{0.9}Gd_{0.1}O_{1.95}$ (GDC10) at relatively lower temperature. TG–DTA of gel formed for other Gd concentrations resulted in the identical observations.

3.2. Fourier transformed infrared (FT-IR) and Raman spectroscopy

FT-IR spectra of GDC10 for as-synthesized, calcined (at 600 °C) and sintered (at 1200 °C) powder is shown in Fig. 2. The features in the IR spectra are bands in the 1200–1700 cm^{-1} (II-region) and 2800–3500 cm^{-1} (III-region) ranges. In addition, the band in the 850–400 cm^{-1} (I-region) range of the IR spectra may be attributed to the characteristic Ce–O vibrations [17]. The bands in the frequency region from 1200 to 1700 cm^{-1} (II-region) are assigned to some traces of un-decomposed nitrates in the as-prepared powder [18] and carbon based impurity species on the unsaturated CeO_2 surface [19].

The band at 1384 cm^{-1} might be due to some traces of remnant nitrates [18]. The band at around 1600 cm^{-1} is due to CO_2. The bands at 1536 and 1416 cm^{-1} are due to asymmetric and symmetric stretching frequency of COO^-. The C–H stretching mode is also observed in the region 2800–3000 cm^{-1}. Moreover, residual water is detected with a large band around 3427 cm^{-1}, corresponding to the O–H stretching frequency. The less intense peak at 1070 cm^{-1} represents the presence of residual organics in the sample. The intensity of these bands decreases after calcination and sintering. The O–H stretching mode present in the calcined and sintered samples may come from moisture absorbed during testing. The less intense impurity bands in the calcined and sintered samples originate from surface and not from bulk, as confirmed in the XRD analysis.

Fig. 3 depicts the Raman spectra of calcined powder of GDC10. A sharp and intense peak observed at 467 cm^{-1} corresponds to CeO_2 due to F_{2g} symmetry of the cubic phase [20]. In addition to this, two weak peaks are observed at 550 and 600 cm^{-1}. These vibrational modes are connected to the defect spaces related to the oxygen vacancies present in the structure of Gd doped ceria nano-crystalline sample [21]. When Gd is doped in ceria, every two Gd^{3+} substituted for Ce^{4+} makes oxygen ion O^{2-} to leave the lattice in order to keep the electro neutrality (extrinsic oxygen vacancy). According to Nakajima et al. [22] the vibrational states with wave number near the value of 600 cm^{-1} are attributed to the defect spaces including or neighboring of the intrinsic oxygen vacancies, while the mode at 550 cm^{-1} is associated with oxygen vacancies induced by doping CeO_2 with Gd^{3+} (extrinsic vacancies). Further, the absence of the vibrational mode at 360 cm^{-1} corresponding to Gd_2O_3 cubic phase [23] confirms the formation of solid solution at room temperature.

3.3. X-ray diffraction (XRD)

Prepared samples crystallized in fluorite form, as confirmed from the XRD patterns of as-synthesized powders (Fig. 4a). The broad diffraction peaks in the XRD patterns clearly depicts the nano-crystalline nature of as-synthesized powders. The crystallites grow upon calcination at 600 °C but the broadness of peaks is persevered (nano-crystallinity). Fig. 4b shows this effect for GDC10 sample, while upon sintering at 1200 °C the peaks are turned into comparably sharp diffraction peaks. For as-synthesized powders and sintered samples (at 1200 °C) of $Ce_{1-x}Gd_xO_{2-x/2}$ (x = 0–0.30), the crystallite sizes were in the range of 9–17 nm and 40–60 nm, respectively. There was no linear variation in crystallite size with an increase/decrease in Gd concentration.

The absence of Ce_2O_3 reflection peaks in XRD pattern of GDC10 sample sintered at 1200 °C indicates that there was no reduction of Ce^{4+} to Ce^{3+}. However, the (0 0 3) reflection peak due to Ce_2O_3 emerge for GDC10 sample sintered at 1300 °C and become more prominent for higher sintering temperatures (e.g. at 1400 °C—Fig. 4b). The similar trend was also observed for other compositions. Apart from these observations in a similar research [13], however with unique sintering approach, emergence of Ce_2O_3 peaks was not observed even for the samples sintered at 1600 °C. In addition, of unique approach of sintering, the authors have not used any kind of binder during the formation of green samples. Therefore, the emergence of Ce_2O_3 peak, in our case, may be attributed to uncontrolled decomposition of binder during the final sintering.

In general, poly-vinyl alcohol (PVA) is used as binder (organic material) during synthesis of green samples in ceramic route. When these green samples are introduced for thermal treatments, binder undergoes thermal decomposition and evolves voluminous product gases. When such green samples (having binder in its particle matrix) are allowed to sinter at higher temperature, the evolving gases pressurize the surrounding particle matrix and flake out of the sample (formation of pores). However, these pores are filled during further heating process at higher temperatures. These evolving gases sometime block the contact of atmospheric air and particles at higher temperatures, where it could apparently establishes a very low oxygen partial pressure. If the pores (with low oxygen partial pressure) are blocked due to surface grain growth then the low oxygen partial pressure remains trapped in particle matrix. This apparent low oxygen partial pressure and high temperature i.e. greater than 1273 K is a sufficient condition to provide the transition of Ce^{4+} to Ce^{3+}, a well-known behavior of ceria [24].

During the doping of ceria with gadolinia, the large sized Gd^{3+} (radius is 0.1 nm) ions expand the host lattice of ceria (radius is 0.09 nm). This expansion causes uniform strain in the lattice, as the material is elastically deformed. This effect changes the lattice-plane-spacing and the diffraction peak shifts to new '2θ' positions. Therefore, the lattice parameter 'a' of the doped ceria, given by $a = d\sqrt{h^2+k^2+l^2}$ has been observed to increase with an increase in Gd content in ceria. Fig. 5 shows variation of unit cell parameter, a, with dopant content, x, of Gd^{3+} ions. The trend of variation is linear and follows the equation as, $a_{Sint}(x) = 0.062x + 5.409$. According to Vegard's rule, the lattice parameter of a solid solution varies linearly with

Table 2
Grain size and relative density of GDC samples sintered at 1400 °C.

Sample name	Grain size (μm)	Relative density (%)
GDC00	7.675	79
GDC05	5.652	92
GDC10	4.841	94
GDC15	3.023	91
GDC20	1.976	95
GDC25	1.964	94
GDC30	1.960	93

an increase in dopant concentration. Therefore, the prepared samples are confirmed to form solid solution of gadolinia and ceria.

3.4. Scanning electron microscopy (SEM) and relative density measurements

According to solute drag effect [25] in a solid solution, during sintering the dopant segregates at the grain boundary and inhibits the surface and grain boundary diffusion mechanism. Hence, in our case, these restrained mechanisms lead to decelerated grain growth for the samples with higher 'Gd' contents. Variation in average grain size and relative density of GDC samples sintered at 1400 °C is shown in Table 2. From Table 2, a gradual decrease in average grain size is observed, however, this trend stops for doping of 20% Gd in ceria. For the samples with doping contents of 20% and above, the average grain size remains steady. These features can be clearly seen in respective SEM images (Fig. 6a–g). Additionally, the grain size distribution is observed to be broad for $x = 0$ and 0.1 while other samples (for $x \geq 0.15$) showed nearly uniform grains (grain size distribution is narrow).

Apart from these variations with doping concentrations, it is observed that all the samples sintered at 1400 °C showed the formation of relaxed and rounded/spherical shaped grains. However, for the samples sintered at 1200 °C the grains were comparatively smaller than that of respective samples sintered at 1400 °C. Fig. 6h shows typical SEM image of (GDC10) sample sintered at 1200 °C for 8 h. Observed globular shaped grains are of size of 200 nm. Thus, sintering at 1400 °C/8 h led to 24 times larger grains than that of sintered at 1200 °C/8 h. However, this enhanced grain size may show an adverse effect on its electrical performance. In general, the grain size in dense sintered bodies strongly affects mechanical and electrical properties of solid electrolytes. In addition, nano-crystalline samples can lead to the formation of inconsistent dopant or vacancy nano-domains and a large amount of grain boundaries. This large amount of grain boundaries can cause an increase in impurities segregation and thermal ageing of samples. Therefore, the effect of grain size on the physical and chemical properties of submicrometer polycrystalline bodies is expected to be more significant than those of normal polycrystalline bodies with grain size of several micrometers.

Particularly, for GDC10 samples sintered at 1200 °C for 8 and 12 h had shown relative densities of 93% and 95%, respectively while for samples sintered at 1400 °C it was 95%. Thus, the density of samples is saturated at 1200 °C and further grain growth is progressed by surface and/or grain boundary diffusion mechanism (non-densification processes) for higher sintering temperature.

4. Conclusions

GDC nano-powders have been synthesized using single-step glycine–nitrate process (GNP). Raman and FT-IR analysis of as-synthesized and calcined powders confirms the formation of phase-pure GDC solid solution instead of a CeO_2 and Gd_2O_3 mixture. To synthesize highly dense GDC ceramic bodies the green bodies should be prepared either using an organic binder with consequent pre-sintering step or should be prepared without binder.

Acknowledgements

The authors are thankful to UGC-DAE-IUC, Indore, and DRDO, New Delhi, for financial assistance. We would like to acknowledge Dr. D. Phase, UGC-DAE IUC Indore for extending SEM characterization facilities. Dr. M.G. Chourashiya is thankful to CSIR, New Delhi, for a senior research fellowship.

References

[1] H. Inaba, H. Tagawa, Solid State Ionics 83 (1996) 1–16.
[2] H. Abdul, Y. Iskandar, Catal. Today 96 (2004) 165–170.
[3] M. Fathi, E. Bjorgum, O.A. Rokstad, Catal. Lett. 72 (2001) 25–31.
[4] P. Jasinski, T. Suzuki, H.A. Anderson, Sens. Actuators B 95 (2003) 73–77.
[5] R. Li, S. Yabe, M. Yamashita, S. Momose, S. Yoshida, S. Yin, T. Sato, Solid State Ionics 151 (2002) 235–241.
[6] S. Wang, H. Inaba, H. Tagawa, T. Hashimoto, J. Electrochem. Soc. 144 (1997) 4076–4080.
[7] N. Maffei, A.K. Kuriakose, Solid State Ionics 107 (1998) 67–71.
[8] I. Riess, D. Braunshtein, D.S. Tannhause, J. Am. Ceram. Soc. 64 (1981) 479–485.
[9] A.L. Dragoo, C.K. Chiang, in: F. Salzano (Ed.), Proc. Conf. on High Temperature Solid Oxide Electrolytes, Brookhaven National Laboratory, Upton, USA, 1983, pp. 268–281.
[10] J. Van Herle, T. Horita, T. Kawada, N. Sakai, H. Yokokawa, M. Dokiya, Solid State Ionics 86–88 (1996) 1255–1258.
[11] S.J. Hong, K. Mehta, A.V. Virkar, J. Electrochem. Soc. 145 (1998) 638–647.
[12] K. Yamashita, K.V. Ramanujachary, M. Greenblatt, Solid State Ionics 81 (1995) 53–60.
[13] V. Espositow, E. Traversa, J. Am. Ceram. Soc. 91 (2008) 1037–1051.
[14] L.D. Jadhav, M.G. Chourashiya, K.M. Subhedar, A.K. Tyagi, J.Y. Patil, J. Alloys Compd. 470 (2009) 383–386.
[15] M.M.A. Sekar, S.S. Manoharan, K.C. Patil, J. Mater. Sci. Lett. 9 (1990) 1205–1206.
[16] S.T. Aruna, M. Muthuraman, K.C. Patil, Solid State Ionics 111 (1998) 45–51.
[17] T. Wang, D.C. Sun, Mater. Res. Bull. 43 (2008) 1754–1760.
[18] K. Nakamoto, Infrared and Raman Spectra of Inorganic and Coordination Compounds, 2nd ed., Wiley, New York, 1997.
[19] V. Bolis, G. Magnacca, G. Cerrato, C. Morterra, Thermochim. Acta 379 (2001) 147–161.
[20] J. Matta, D. Courcot, E. Abi-aad, A. Aboukays, Chem. Mater. 14 (2002) 4118–4125.
[21] Z.D. Dohcevic-Mitrovic, M. Grujic-Brojcin, M. Scepanovic, Z.V. Popovic, S. Boskovic, B. Matovic, M. Zinkevich, F. Aldinger, J. Phys.: Condens. Matter 18 (2006) S2061–S2068.
[22] A. Nakajima, A. Yoshihara, M. Ishigame, Phys. Rev. B 50 (1994) 13297–13307.
[23] A. Garcia-Murillo, C. Le Luyer, C. Garapon, C. Dujardin, E. Bernstein, C. Pedrini, J. Mugnier, Opt. Mater. 19 (2002) 161–168.
[24] M.G. Chourashiya, J.Y. Patil, S.H. Pawar, L.D. Jadhav, Mater. Phys. Chem. 109 (2008) 39–44.
[25] H. Inaba, T. Nakajima, H. Tagawa, Solid State Ionics 106 (1998) 263–268.